Journal of Catalysis 307 (2013) 55–61

Contents lists available at SciVerse ScienceDirect

Journal of Catalysis

journal homepage: www.elsevier.com/locate/jcat

Highly recoverable organoruthenium-functionalized mesoporous silica boosts aqueous asymmetric transfer hydrogenation reaction

Rui Liu, Tanyu Cheng, Lingyu Kong, Chen Chen, Guohua Liu *, Hexing Li *

Key Laboratory of Resource Chemistry of Ministry of Education, Shanghai Key Laboratory of Rare Earth Functional Materials, Shanghai Normal University, Shanghai 200234, PR China

ARTICLE INFO

Article history:
Received 18 May 2013
Revised 28 June 2013
Accepted 9 July 2013

Keywords:
Asymmetric transfer hydrogenation
Heterogeneous catalysis
Immobilization
Mesoporous materials

ABSTRACT

Exploring functionalized mesoporous silica to achieve enhanced catalytic activity and enantioselectivity in heterogeneous asymmetric catalysis presents a significant challenge that is critical for understanding the function of support and controlling chiral complexation behavior. In this contribution, by cooperative assembly of chiral 4-(trimethoxysilyl)ethyl)phenylsulfonyl-1,2-diphenylethylene-diamine and tetraethoxysilane followed by complexation with organoruthenium complex, we report a unique three-dimensional chiral organoruthenium-functionalized chrysanthemum-like mesoporous silica (CMS). As demonstrated in the studies, taking advantage of the active site-isolated chiral organoruthenium catalytic nature, this heterogeneous catalyst ArRuTsDPEN-CMS (Ar = hexamethylbenzene, TsDPEN = 4-methylphenylsulfonyl-1,2-diphenylethylene-diamine) displays enhanced catalytic activity and enantioselectivity in aqueous asymmetric transfer hydrogenation with extensive substrates. Furthermore, this heterogeneous catalyst can be conveniently recovered and reused at least 10 times without loss of its catalytic efficiency. These features render this catalyst particularly attractive in practice of organic synthesis in an environmentally friendly manner. Also, this outcome from the study clearly shows that the strategy described here offers a general approach to immobilization of chiral ligand-derived silane onto a functionalized mesoporous material with significant improving catalytic activity.

1. Introduction

During the past few years, three-dimensional flowerlike mesoporous silicas have emerged as an interesting class of hybrid materials with potential applications in catalysis, drug delivery, and bimolecular separations [1,2]. Like traditional mesoporous silica materials as immobilized supports to anchor various chiral complexes [3–9], these flowerlike mesoporous silicas do also possess large specific surface area/pore volume, tunable pore dimension/well-defined pore arrangement, and high mechanical stability. These features can serve as a potential immobilized platform to assemble desired chiral functionality for design of various chiral heterogeneous catalysts. Unlike traditional mesoporous silica materials, typical three-dimensional flowerlike mesoporous silica has relatively short nanochannel of nanopore and special cavum of flower, which offers easy accessibility/diffusion of substrates to accelerate reaction rate. In particular, novel cooperative assembly approach can construct uniformly distributive active center within its silicate network, which is beneficial to mimic homogeneous catalytic environment and simplify the elucidation of catalytic mechanism [1,10]. More importantly, unique self-assembly process often requires cetyltrimethylammonium bromide (CTAB) as a structure-directing template agent, in which the residual CTAB within its silicate network can offer as an additional phase-transfer function and can facilitate a two-phase asymmetric reaction that has not been recognized yet. Thus, choosing a typical two-phase asymmetric transfer hydrogenations reaction catalyzed by N-sulfonylated diamine-based organometallic complexes [11–15] and taking advantage of the significant benefits of this kind of functionalized mesoporous silica, it is highly expected that excellent catalytic activity and enantioselectivity in aqueous asymmetric transfer hydrogenation reaction can be obtained by controlling the active site-isolated complexation behavior, although this has not been explored yet in asymmetric catalysis.

As a part of the program aimed at developing highly recoverable heterogeneous catalysts [16–23], in this contribution, we report a chiral organoruthenium-functionalized chrysanthemum-like mesoporous silica (CMS), which consists of residual CTAB functionality and chiral diamine-based organoruthenium functionality within its silicate network. As expected, as a functionalized heterogeneous catalyst: ArRuTsDPEN-CMS [24] (Ar = hexamethylbenzene, TsDPEN = 4-methylphenylsulfonyl-1,2-diphenylethylene-diamine), it does not only greatly enhance the catalytic performance but also improve the enantioselective performance in aqueous asymmetric

* Corresponding authors.
E-mail addresses: ghliu@shnu.edu.cn (G. Liu), hexing-li@shnu.edu.cn (H. Li).

0021-9517/$ - see front matter © 2013 Elsevier Inc. All rights reserved.
http://dx.doi.org/10.1016/j.jcat.2013.07.007

transfer hydrogenation. Moreover, this organoruthenium-functionalized chrysanthemum-like mesoporous silica can serve as a general catalyst to promote asymmetric transfer hydrogenation for extensive substrates including various aryl ketones and quinolines in aqueous medium. In addition, this robust catalyst can be readily recycled and reused at least 10 times without reducing its catalytic efficiency, presenting a practical application in asymmetric synthesis.

2. Experimental

2.1. Characterization

Ru loading amount in the catalyst was analyzed using an inductively coupled plasma optical emission spectrometer (ICP, Varian VISTA-MPX). Fourier transform infrared (FTIR) spectra were collected on a Nicolet Magna 550 spectrometer using KBr method. X-ray powder diffraction (XRD) was carried out on a Rigaku D/Max-RB diffractometer with Cu Kα radiation. Scanning electron microscopy (SEM) images were obtained using a JEOL JSM-6380LV microscope operating at 20 kV. Transmission electron microscopy (TEM) images were performed on a JEOL JEM2010 electron microscope at an acceleration voltage of 220 kV. X-ray photoelectron spectroscopy (XPS) measurements were performed on a PerkinElmer PHI 5000C ESCA system. A 200 μm diameter spot size was scanned using a monochromatized Aluminum Kα X-ray source (1486.6.6 eV) at 40 W and 15 kV with 58.7 eV pass energies. All the binding energies were calibrated by using the contaminant carbon (C_{1s} = 284.6 eV) as a reference. Nitrogen adsorption isotherms were measured at 77 K with a Quantachrome Nova 4000 analyzer. The samples were measured after being outgassed at 423 K overnight. Pore size distributions were calculated by using the BJH model. The specific surface areas (S_{BET}) of samples were determined from the linear parts of BET plots (p/p_0 = 0.05–1.00). Thermal gravimetric analysis (TGA) was performed with a PerkinElmer Pyris Diamond TG analyzer under air atmosphere with a heating ramp of 5 K/min. Solid-state NMR experiments were explored on a Bruker AVANCE spectrometer at a magnetic field strength of 9.4 T with ^{1}H frequency of 400.1 MHz, ^{13}C frequency of 100.5 MHz, and ^{29}Si frequency of 79.4 MHz with 4 mm rotor at two spinning frequency of 5.5 kHz and 8.0 kHz, TPPM decoupling is applied in the during acquisition period. ^{1}H cross-polarization in all solid-state NMR experiments was employed using a contact time of 2 ms and the pulse lengths of 4 μs. Elemental analysis was performed with a Carlo Erba 1106 Elemental Analyzer.

2.2. Catalyst preparation

2.2.1. Preparation of TsDPEN-functionalized CMS (*4*)

In a typical synthesis, 8.0 mL H_2O, 40.0 mL ethyl ether, and 1.0 mL ammonia solution (25–28%) were added in a closed vessel and vigorously stirred at ambient temperature. When the solution became homogeneous, 2.0 mL (8.06 mmol) TEOS was dropwise added and stirred continuously for 3 h. Then to this, solution was added 1.0 g CTAB (2.74 mmol) and a mixture solution of TEOS (2.0 mL, 8.06 mmol) and (*R*,*R*)-TsDPEN-derived silica (**3**) (0.80 g, 1.60 mmol). The resulting mixture was vigorously stirred for 12 h at ambient temperature. The products were collected by centrifugating, washing repeatedly for three times with distilled water. The surfactant was then extracted by refluxing with HCl–ethanol solution for 12.0 h. After Soxhlet extraction in dry CH_2Cl_2 to remove unreacted start materials, the solid was dried under reduced pressure overnight to afford TsDPEN-functionalized CMS (**4**) (1.22 g) as a white powder. IR (KBr) cm^{-1}: 3449.2 (s), 2928.8 (w), 2856.7 (w), 1632.1 (m), 1496.5 (w), 1457.9 (w), 1082.2 (s), 955.3 (m), 798.5 (m), 702.2 (w), 568.0 (w), 462.1 (m); ^{29}Si MAS/NMR (79.4 MHz): T^3 (δ = −68.4 ppm), Q^2 (δ = −92.6 ppm), Q^3 (δ = −101.7 ppm), Q^4 (δ = −110.9 ppm); ^{13}C CP/MAS (100.5 MHz): 8.3–20.8 (<u>C</u>H_3 in C_6Me_6, Si<u>C</u>H_2 and <u>C</u>H_3 of CTAB), 24.0–34.3 (<u>C</u>H_2Ph and <u>C</u>H_2 of CTAB), 52.8 (N<u>C</u>H_2 and N<u>C</u>H_3 of CTAB), 55.6–65.1 (N<u>C</u>HPh of T_SDPEN), 119.7–141.4, 148.7 (<u>C</u> of Ph and Ar) ppm; Elemental analysis (%): C 11.72, H 2.15, N 1.01, S 0.76.

2.2.2. Preparation of ArRuTsDPEN-CMS (*5*)

In a typical synthesis, to a stirred suspension of **4** (1.0 g) and NEt_3 (1.00 mL, 16.5 mmol) in 20 mL dry CH_2Cl_2 was added [$RuCl_2$(C_6Me_6)]$_2$ (0.11 g, 0.16 mmol). The resulting mixture was stirred at room temperature for 24 h. Then, the residues were filtrated and washed twice with 20 mL of dry CH_2Cl_2. After Soxhlet extraction in dry CH_2Cl_2 to remove unreacted start materials, the solid was dried under reduced pressure overnight to afford the catalyst **5** (1.02 g) as a light yellow powder. ICP analysis showed that the Ru loading amount was 27.12 mg (0.266 mmol) per gram catalyst. IR (KBr) cm-1: 3424.4 (s), 2928.4 (w), 2855.6 (w), 1630.1 (m), 1498.3 (w), 1457.9 (w), 1384.0 (w), 1082.1 (s), 953.1 (m), 801.2 (m), 699.6 (w), 565.2 (w), 462.2 (m); S_{BET}: 578.3 m^2/g, V_{pore}: 0.74 cm^3/g, d_{pore}: 3.73 nm; ^{29}Si MAS/NMR (79.4 MHz): T^3 (δ = −67.8 ppm), Q^2 (δ = −92.5 ppm), Q^3 (δ = −101.8 ppm), Q^4 (δ = −111.0 ppm); ^{13}C CP/MAS (100.5 MHz): 8.8–21.4 (<u>C</u>H_3 in C_6Me_6, Si<u>C</u>H_2 and <u>C</u>H_3 of CTAB), 24.0–33.4 (<u>C</u>H_2Ph and <u>C</u>H_2 of CTAB), 52.8 (N<u>C</u>H_2 and N<u>C</u>H_3 of CTAB), 55.6–64.3 (N<u>C</u>HPh of T_SDPEN), 89.8 (<u>C</u>$_6$ of C_6Me_6), 121.3–141.9, 149.5 (<u>C</u> of Ph and Ar) ppm; Elemental analysis (%): C 16.54, H 2.86, N 1.10, S 0.86.

2.3. General procedure for asymmetric transfer hydrogenation

For asymmetric transfer hydrogenation of ketones, the catalyst **5** (15.0 mg, 4.0 μmol of Ru based on the ICP analysis), HCO_2Na (0.27 g, 10.0 mmol), ketone (0.40 mmol), and 2.0 mL of water were added in a 10 mL round bottom flask in turn. The mixture was allowed to react at 40 °C for 3.0–9.0 h. [For asymmetric transfer hydrogenation of quinolines, the catalyst **5** (15.0 mg, 4.0 μmol of Ru based on the ICP analysis), HCO_2Na (0.27 g, 10.0 mmol), quinolines (0.40 mmol), and 2.0 mL (2.0 M HCOOH/HCOONa buffer solution, pH = 5.0) were added in a 10 mL round bottom flask in turn. The mixture was allowed to react at 40 °C for 10.0–24 h.] During that time, the reaction was monitored constantly by TLC. After completion of the reaction, the catalyst was separated via centrifuge (10,000 r/min) for the recycle experiment. The aqueous solution was extracted by Et_2O (3 × 3.0 mL). The combined Et_2O was washed with brine twice and dehydrated with Na_2SO_4. After the evaporation of Et_2O, the residue was purified by silica gel flash column chromatography to afford the desired product. The conversion could be determined by an external standard method, and the ee value could be determined by chiral GC using a Supelco β-Dex 120 chiral column (30 m × 0.25 mm (i.d.), 0.25 μm film) or a HPLC analysis with a UV–Vis detector using a Daicel OJ-H/OD-H/OB-H chiralcel column (Φ 0.46 × 25 cm).

3. Results and discussions

3.1. Syntheses and characterizations of the catalysts

The incorporation of chiral ArRuTsDPEN functionality within its CMS silicate network, abbreviated as ArRuTsDPEN-CMS (**5**), was prepared as outlined in Scheme 1. Firstly, a microemulsion (**2**) was formed in a mixture solvents of $NH_3{\cdot}H_2O$, ethyl ether, and tetraethoxysilane (TEOS **1**) to provide the growing silica seeds. The cooperative assembly and continuous grown between TEOS and 4-(trimethoxysilyl)ethyl)phenylsulfonyl-1,2-diphenyl-

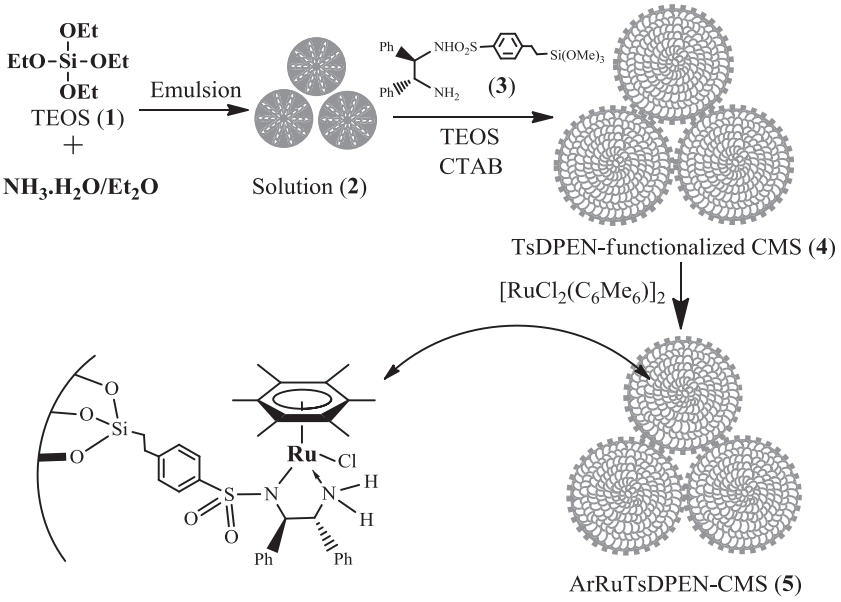

Scheme 1. Immobilization of ArRuTsDPEN within tits silicate network.

ethylene-diamine (**3**) using CTAB as a structure-directing template then afforded chiral TsDPEN-functionalized CMS (**4**) in formation of a white powder. Finally, the chiral organoruthenium-functionalized ArRuTsDPEN-CMS (**5**) was obtained successfully by direct complexation with $[RuCl_2(C_6Me_6)]_2$ followed by thoroughly Soxhlet extraction for clearance of its nanopores (see SI in Figs. S1–3). The inductively coupled plasma (ICP) optical emission spectrometer analysis showed that Ru loading was 27.12 mg (0.266 mmol) per gram catalyst, while the elemental analysis disclosed that the mole amount of S was 0.268 mmol per gram of catalyst calculated from mass % of S atoms (S 0.86%), in which the 1:1 mol ratio of Ru/S suggested generating the well-defined single-site ArRuTsDPEN active center within its silicate network.

The silicate framework, well-defined ArRuTsDPEN active center, and its composition could be confirmed by solid-state CP/MAS NMR spectra, X-ray photoelectron spectroscopy (XPS) and thermal gravimetric (TG/DTA) analysis. As shown in Fig. 1, the ^{29}Si CP/MAS NMR spectra showed that the TsDPEN-functionalized CMS (**4**) and the catalyst **5** presented two groups of typical signals (Q- and T-series) distributed broadly from −50 to −150 ppm as marked in their spectra, in which Q signals are attributed to silica matrix while T signals are corresponding to organosilica. As compared with these typical isomer shift values in the literature (−91.5/−101.5/−110 ppm for $Q^2/Q^3/Q^4$ signals {$[(HO)_2Si(OSi)_2]/[(HO)Si(OSi)_3]/[Si(OSi)_4]$} and −48.5/−58.5/−67.5 ppm for $T^1/T^2/T^3$ signals {$[R(HO)_2SiOSi]/[R(HO)Si(OSi)_2]/[RSi(OSi)_3]$}) [25], it was found easily that the catalyst **5** showed one T^3 peak in T-series and three Q peaks in Q-series, in which only T^3 peak and the strongest Q^3 peak suggested that the catalyst **5** possessed inorganosilicate framework of $(HO)Si(OSi)_3$ with the organosilicate $RSi(OSi)_3$ (R = ArRuTsDPEN functionality) as its main part of silica wall [26].

The ^{13}C CP/MAS NMR spectra clearly demonstrated the formation of well-defined single-site ArRuTsDPEN active center within its CMS silicate network. As shown in Fig. 2, the catalyst **5** displayed the characteristic peaks of chiral TsDPEN moiety, in which the peaks around 55–65 ppm were corresponding to the C atoms of –NCHPh groups. In addition, the characteristic peaks around 128 ppm were corresponded to the C atoms in the Ph groups that were derived from the chiral TsDPEN moiety. As compared the TsDPEN-functionalized-CMS (**4**) with the catalyst **5**, the new appeared peaks around 90 ppm [27] were corresponded to the C atoms in C_6Me_6 rings, while the obviously enhanced peaks around 15 ppm relative to that in the TsDPEN-functionalized-CMS (**4**) were attributed to the additional C atoms of CH_3 groups connected to aromatic rings, suggesting that the complexation of $[RuCl_2(C_6Me_6)]_2$ moiety

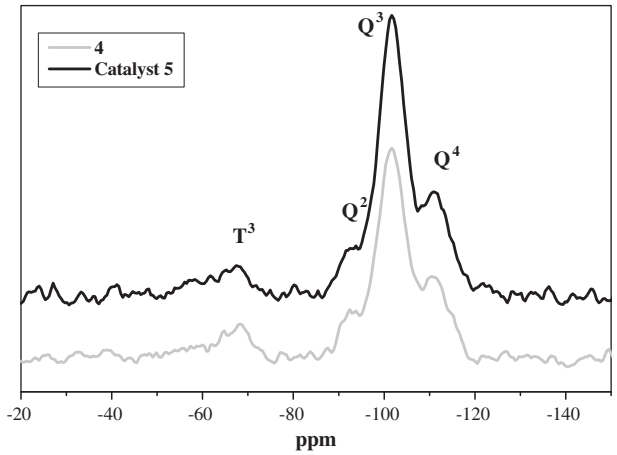

Fig. 1. Solid-state ^{29}Si CP/MAS NMR spectra of **4**–**5**.

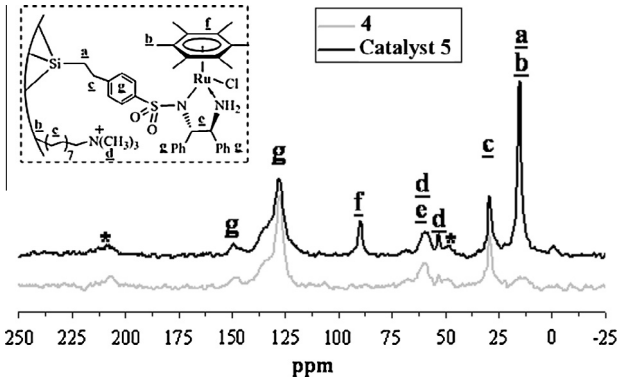

Fig. 2. Solid-state ^{13}C CP/MAS NMR spectra of **4**–**5**.

with chiral ligand was formed. In sharp contrast to these chemical shift values with its homogeneous counterpart ArRuTsDPEN [27], it was found that the catalyst **5** was strongly similar to its homogeneous counterpart, demonstrating that the catalyst **5** had the same well-defined single-site active center as its homogeneous counterpart. This result could be further confirmed XPS investigation as shown in Fig. 3, in which the catalyst **5** showed the same Ru $3d_{5/2}$ electron binding energy as its homogeneous counterpart (281.0 eV versus 281.2 eV) [28], further confirming its well-defined single-site ArRuTsDPEN active center within its silicate network [29,30]. In particular, the carbon signals for the residual CTAB functionality could be observed clearly. The peaks around 30 ppm were ascribed to the C of methylene groups without connection to nitrogen atom in CTAB molecule, and the peaks around 53 ppm were belonged to the C atoms of methyl (or methylene) groups connected to nitrogen atom in CTAB molecule as marked in Fig. 2. These observed peaks suggested that the residual CTAB molecules were incorporated within its CMS silicate network, which could be proved by thermal gravimetric (TG/DTA) analysis discussed below. Furthermore, the other peaks denoted by asterisks were the rotational sidebands that often appeared in the CP/MAS high-speed rotation process [31].

In addition, the contents of ArRuTsDPEN functionality within its silicate network could also be determined by the TG/DTA curves. As shown in Fig. 4, it was found that an endothermic peak around 350 K with weight loss of 13.5% could be attributed to the release of physical adsorption water. The other comprehensive exothermic peaks around 641 K could be assigned to the oxidation of organic molecules (including ArRuTsDPEN and the residual CTAB surfactant), in which the total weight loss was 24.4% when subtracted the contribution of water. In sharp contrast to 8.8% weight loss of the residual CTAB for the pure CMS material (see SI in Fig. S2 and explanation) [32], it was found that 15.6% of ArRuTsDPEN functionality was anchored within its silicate network that was closely consistent with 27.12 mg (0.266 mmol) of Ru loading per gram catalyst detected ICP analysis.

The morphology, pore structure, and ruthenium distribution are further investigated using nitrogen adsorption–desorption technique and scanning electron microscopy (SEM) with chemical mapping technique. As shown in Fig. 5, the nitrogen adsorption–desorption isotherm of the catalyst **5** presented a typical IV character with an H3 hysteresis loop, disclosing that this silicate network was composed of aggregates of sheet-like particles forming slit-shape pores. This behavior was strongly similar to that of the pure CMS material [1], indicating that the cooperative assembly of the chiral functionality within this CMS silicate network was constructed steadily. In addition, SEM images revealed that the

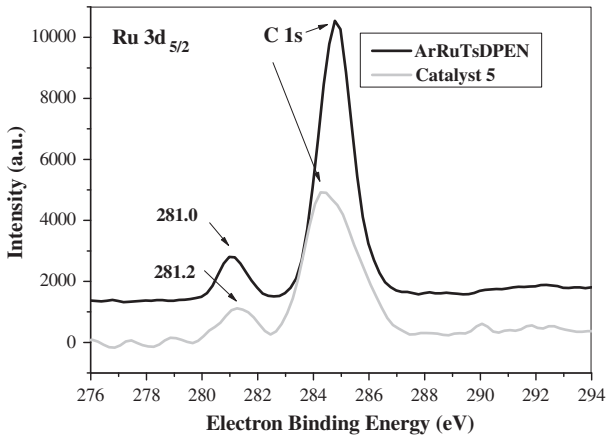

Fig. 3. XPS spectra of the homogeneous ArRuTsDPEN and the catalyst **5**.

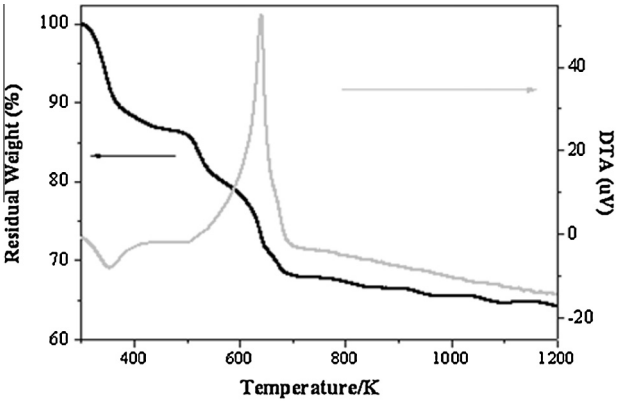

Fig. 4. TG/DTA curves of the catalyst **5**.

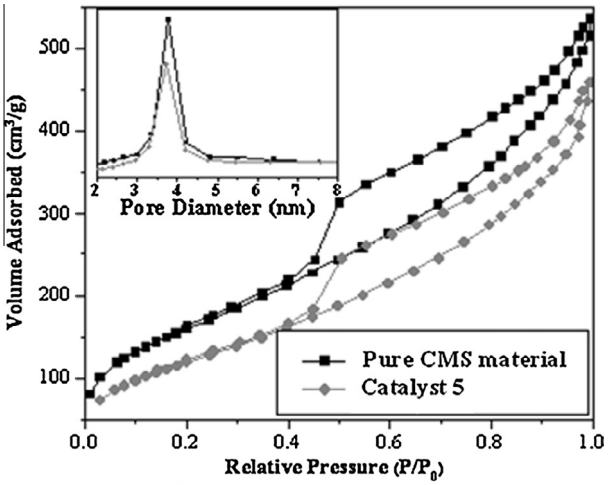

Fig. 5. Nitrogen adsorption–desorption isotherms of the pure CMS material and the catalyst **5**.

catalyst **5** was composed of the uniformly distributed spherical flowers with a particle size of about 750 nm, in which the spherical flowers were constructed over the stacking leaf-shaped nanoflakes as building block (Fig. 6a and b). In particular, the SEM image with a chemical mapping technique indicated that the ruthenium active centers were uniformly distributive within its silicate network (Fig. 6c).

Based on the above characterizations and analyses, a safely conclude could be drawn, in which chiral organoruthenium-functionalized chrysanthemum-like mesoporous silica with inorganosilicate network of $(HO)Si(OSi)_3$, the well-defined single-site ArRuTsDPEN active center, the certain CTAB functionality, and the uniformly distributed ruthenium active centers could be readily constructed *via* cooperative assembly of the chiral silane in its silicate network.

3.2. Catalytic performance of the heterogeneous catalyst

3.2.1. Catalysts screen and catalytic property

As a type of highly active catalysts, homogeneous chiral N-sulfonylated diamine-based η^5-Cp*–M complexes (η^5-Cp* = -pentamethyl cyclopentadiene) and η^6-arene–M complexes (η^6-arene = benzene or hexamethylbenzene) (M = Ru, Rh, and Ir) are used extensively in aqueous asymmetric transfer hydrogenation of ketones [11,12], and some successful examples for immobilization of homogeneous ruthenium complexes have exhibited excellent enantioselectivities for various asymmetric reactions

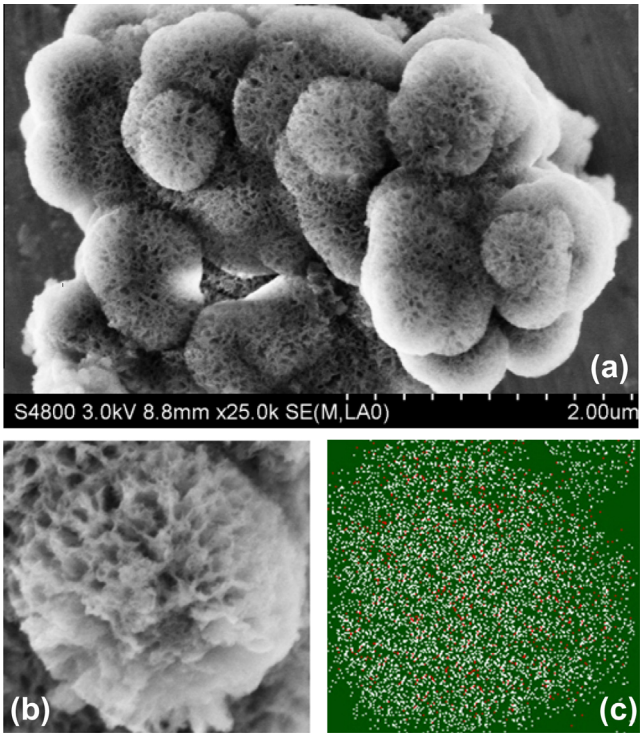

Fig. 6. (a) SEM image of **5**, and (b and c) a chemical mapping of **5** showing the distribution of Si (white) and Ru (red). (For interpretation of the references to color in this figure legend, the reader is referred to the web version of this article.)

[33–36]. In this case, chiral TsDPEN-functionalized CMS (**4**) was screened *via* the complexation with those extensively studied organometallic $[Cp^*MCl_2]_2$ and $[ArMCl_2]_2$ (M = Ru, Rh and Ir) in an aqueous HCOONa system, respectively. However, in most cases, their enantioselectivities were lower than their corresponding homogenous counterparts (see SI in Fig. S4). To our delight, only in the case of $[RuCl_2(C_6Me_6)]_2$, it was found that a slightly enhanced enantioselectivity relative to its homogenous counterpart could be obtained. As a result, ArRuTsDPEN-CMS (**5**) was identified as an optimal heterogeneous catalyst in this asymmetric reaction.

Due to the typical two-phase catalysis system in this asymmetric transfer hydrogenation reaction, it often needs Bu_4NBr acting as a phase-transfer catalyst to enhance its catalytic efficiency. In this case, because of the presence of the residual CTAB functionality, this asymmetric transfer hydrogenation catalyzed by the catalyst **5** was investigated in the absence of Bu_4NBr system, in which HCO_2Na worked as a hydrogen source and 1.0% mol of CMS silica acted as a catalyst according to the reported methods [13]. As shown in Table 1, the excellent conversions, no side products, and high enantioselectivities were obtained for all tested substrates. Moreover, it was noteworthy that the electronic properties of substituents at acetophenones did not affect significantly its enantioselectivity as its homogeneous behavior, in which the asymmetric reactions with electron-rich and electron-poor substituents at acetophenones were equally efficient (entries 4–13).

3.2.2. Nature of the heterogeneous catalysis

More attractively, in all cases, it was found that the catalyst **5** presented the obviously high catalytic activity relative to its homogeneous counterpart under the same reaction condition. Taking acetophenone as an example, the catalyst **5** within 3.0 h gave (*S*)-1-phenyl-1-ethanol with more than 99% conversion, which was higher than 91% of its homogeneous counterpart (entry 1 versus entry 1 in bracket). This behavior was more noticeable in cases of 4-methylacetophenone and 4-methoxylacetophenone because

Table 1
5-Catalyzed enantioselective transfer hydrogenation of aromatic methyl ketones.[a]

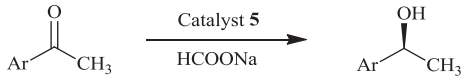

Entry	Ar	Time	% con[b]	% ee[b]
1	Ph	3	>99 (91)	98 (98)[c]
2	Ph	3	>99	98[d]
3	Ph	3	94	98[e]
4	4-FPh	3	>99	99
5	4-ClPh	3	>99	98
6	4-BrPh	3	>99	96
7	3-BrPh	3	>99	98
8	4-MePh	6	>99(70)	97 (95)[c]
9	4-OMePh	12	97 (67)	99 (98)[c]
10	3-OMePh	3	>99	99
11	4-CNPh	3	99	88
12	4-NO_2Ph	3	99	90
13	4-CF_3Ph	3	99	95
14	2-Naphthyl	4	>99	98

[a] Reaction conditions: catalyst **5** (15.00 mg, 4.00 μmol of Ru based on the ICP analysis), HCO_2Na (0.27 g, 10.0 mmol), ketone (0.40 mmol), 2.0 mL water, reaction temperature (40 °C), and reaction time (3.0–12.0 h).
[b] Determined by chiral GC or HPLC analysis (see SI in Fig. S6).
[c] Data in the bracket were obtained using ArRuTsDPEN as a catalyst in absence of Bu_4NBr system.
[d] Data were obtained using the pure CTAB plus ArRuTsDPEN as a catalyst.
[e] Data were obtained using the pure CMS material plus ArRuTsDPEN as a catalyst.

of their intrinsic longer reaction time in homogeneous catalysis system (entries 8–9 in Table 1) [13]. In order to confirm this judgment, one kinetic profile in the asymmetric reaction of 4-methylacetophenone catalyzed by the catalyst **5** and its homogeneous counterpart ArRuTsDPEN had been investigated (see SI Fig. S5). It was found that the catalyst **5** had a higher initial activity than its homogeneous ArRuTsDPEN, in which the initial TOFs within 1.0 h was 351.5 versus 234.0 mol mol^{-1} h^{-1}. As expected, the catalyst **5** could increase significantly catalytic performance in a phase-transfer function in aqueous medium.

In order to explore the nature of this heterogeneous catalysis, two parallel experiments using pure CTAB molecule plus its homogeneous ArRuTsDPEN (the former) or the pure CMS material plus its homogeneous ArRuTsDPEN (the latter) as catalysts were investigated. The results showed that the former afforded the corresponding alcohol with more than 99% conversion and 98% ee (entry 2), while the latter gave the alcohol with 94% conversion and 98% ee (entry 3). In the former case, the asymmetric reaction afforded the same conversion and ee value as the catalyst **5** (entry 2 versus entry 1), demonstrating that CTAB molecule did also promote the catalytic performance. The latter case indicated that the homogeneous catalyst *via* non-covalent adsorption could result in a comparable catalytic performance. However, when this catalyst in the latter case was undergone a process of Soxhlet extraction, the reused catalyst gave only tiny products, demonstrating that the nature of this heterogeneous catalysis was indeed derived from the heterogeneous catalyst itself rather than homogeneous catalyst derived from the non-covalent physical adsorption since the catalyst **5** had been treated with through this process of Soxhlet extraction.

3.2.3. Scope of 5-catalyzed asymmetric transfer hydrogenation

In addition to acetophenones, described in Table 1, the catalyst **5** could also be applied to the asymmetric transfer hydrogenation of other aryl ketones including cyclic and acyclic ones in aqueous medium (Table 2). Again, excellent conversions and high enantioselectivities were obtained under the similar reaction condition [13]. It was worth mentioning that bisketones could be reduced

Table 2
5-Catalyzed enantioselective transfer hydrogenation of other aryl ketones.[a]

Entry	Substrate	Product	% conv[b]	% ee[b]
1	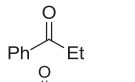		>99	98
2	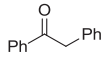	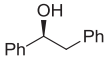	>99	97
3	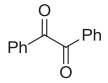	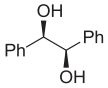	>99	99
4	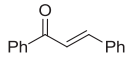	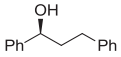	>99	93
5	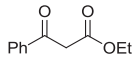	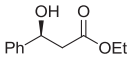	>99	94
6			>99	99
7			95	99
8			>99	98

[a] Reaction conditions: catalyst **5** (15.0 mg, 4.0 μmol of Ru based on the ICP analysis), HCO_2Na (0.27 g, 10.0 mmol), ketone (0.40 mmol), 2.0 mL water, reaction temperature (40 °C), and reaction time (3.0–12.0 h).
[b] Determined by chiral GC or HPLC analysis (see SI in Fig. S7).

Table 3
5-Catalyzed enantioselective transfer hydrogenation of quinolines.[a]

Entry	Substrate	Product	% conv[b]	% ee[b]
1	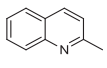		>99	98
2	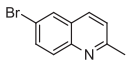	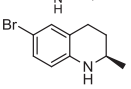	>99	99
3	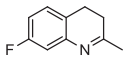	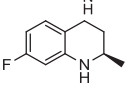	>99	99
4	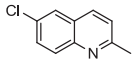	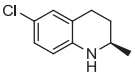	>99	96
5	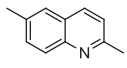	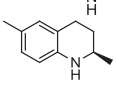	>99	97

[a] Reaction conditions: catalyst **5** (15.0 mg, 4.0 μmol of Ru based on the ICP analysis), HCO_2Na (0.27 g, 10.0 mmol), quinolines (0.40 mmol), 2.0 mL (2.0 M HCOOH/HCOONa buffer solution, pH = 5.0), reaction temperature (40 °C), and reaction time (10.0–12.0 h).
[b] Determined by chiral HPLC analysis (see SI in Fig. S8).

simultaneously with excellent enantioselectivity (entry 3). Moreover, an enone was smoothly transformed into a chiral alcohol in "one-pot" fashion with high catalytic efficiency (entry 4), while the ester moiety could be tolerated in a ketoester (entry 5).

Also, the catalyst **5** could be applied to the asymmetric transfer hydrogenation of quinolines [37,27,38] as shown in Table 3, in which excellent conversions and enantioselectivities were observed [37]. These results shown here demonstrate that the heterogeneous catalyst **5** can serve as a general catalyst for promoting asymmetric transfer hydrogenation with extensive substrates.

3.2.4. Catalyst's stability and recyclability

An important feature for design of any heterogeneous catalyst is the easy separation *via* simple filtration, and the recovered catalyst

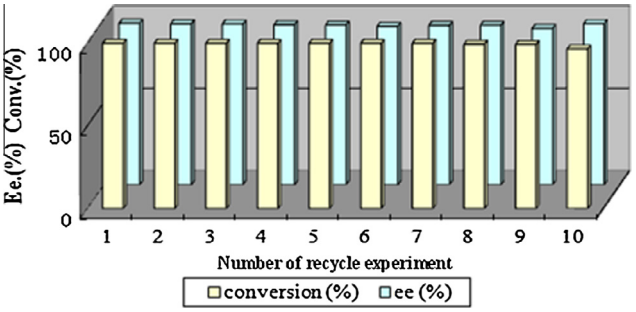

Fig. 7. Reusability of the catalyst **5** using acetophenone as a substrate.

retains its catalytic activity and enantioselectivity after multiple cycles. As shown in Fig. 7, the heterogeneous catalyst **5** was recovered easily and reused repeatedly if acetophenone was chose as a substrate. In ten consecutive reactions, the recycling catalyst **5** still afforded 96% conversion and 97% ee (see SI in Table S1 and Fig. S9). Remarkably, high recyclability should be due to the fact that the high dispersive ArRuTsDPEN active centers *via* strong covalent-bonding immobilization within its CMS silicate network verified by the SEM chemical mapping can decrease efficiently the leaching of Ru. An evidence to support the view came from the ICP analysis, in which the amount of Ru after tenth recycle was 25.85 mg (0.251 mmol) per gram catalyst, and only 5.6% of Ru was lost. Furthermore, this behavior could be further confirmed in the case of the asymmetric reduction 2-methylquinoline, in which the recycling catalyst **5** after ten recycles still afforded 98% conversion and 94% ee, respectively (see SI in Table S2 and Fig. S10).

4. Conclusions

In conclusions, we develop a new strategy for easy immobilization of chiral organoruthenium complex within chrysanthemum-like mesoporous silicate network. Like transitional heterogeneous catalysts, the catalyst **5** can be recovered conveniently and subsequently reused at least 10 times without affecting its catalytic efficiency. Unlike the reported chiral heterogeneous catalysts, the catalyst displays excellent catalytic activity and high enantioselectivity in the aqueous asymmetric transfer hydrogenation reactions with extensive substrates. The outcomes from the study clearly show that the strategy described here offers a general approach to assembly of chiral ligand-derived silane onto a functionalized mesoporous silica with significant improving catalytic performance, which will render the catalyst as a promising promoter for practical application in asymmetric synthesis.

Acknowledgments

This study was supported by China National Natural Science Foundation (20673072), Shanghai Sciences and Technologies Development Fund (10DJ1400103, 10JC1412300 and 12nm0500500), CSIRT (IRT1269) and Shanghai Municipal Education Commission (12ZZ13).

Appendix A. Supplementary material

Supplementary data associated with this article can be found, in the online version, at http://dx.doi.org/10.1016/j.jcat.2013.07.007.

References

[1] H.J. Zhang, Z.Y. Li, P.P. Xu, R.F. Wu, Z. Jiao, Chem. Commun. 46 (2010) 6783.
[2] M.E. Davis, Nature 417 (2002) 813.

[3] F. Kleitz, Handbook of Asymmetric Heterogeneous Catalysis, Wiley-VCH, Weinheim, 2008. pp. 178.
[4] D.E. De Vos, M. Dams, B.F. Sels, P.A. Jacobs, Chem. Rev. 102 (2002) 3615.
[5] S. Minakata, M. Komatsu, Chem. Rev. 109 (2009) 711.
[6] M. Bartók, Chem. Rev. 110 (2010) 1663.
[7] A. Mehdi, C. Reye, R. Corriu, Chem. Soc. Rev. 40 (2011) 563.
[8] H.Q. Yang, L. Zhang, L. Zhong, Q.H. Yang, C. Li, Angew. Chem., Int. Ed. 46 (2007) 6861.
[9] J.M. Thomas, R. Raja, Acc. Chem. Res. 41 (2008) 708.
[10] L. Zhang, Y.N. Guo, J. Peng, X. Liu, P. Yuan, Q.H. Yang, C. Li, Chem. Commun. 47 (2011) 4087.
[11] T. Ikariya, A.J. Blacker, Acc. Chem. Res. 40 (2007) 1300.
[12] R. Malacea, R. Poli, E. Manoury, Coord. Chem. Rev. 254 (2010) 729.
[13] X.F. Wu, X.H. Li, A. Zanotti-Gerosa, A. Pettman, J. Liu, A.J. Mills, J.L. Xiao, Chem. Eur. J. 14 (2008) 2209.
[14] P.N. Liu, J.G. Deng, Y.Q. Tu, S.H. Wang, Chem. Commun. (2004) 2070.
[15] C. Wang, C.Q. Li, X.F. Wu, A. Pettman, J.L. Xiao, Angew. Chem., Int. Ed. 48 (2009) 6524.
[16] H.S. Zhang, R.H. Jin, H. Yao, S. Tang, J.L. Zhuang, G.H. Liu, H.X. Li, Chem. Commun. 48 (2012) 7874.
[17] W. Xiao, R.H. Jin, T.Y. Cheng, D.Q. Xia, H. Yao, F. Gao, B.X. Deng, G.H. Liu, Chem. Commun. 48 (2012) 11898.
[18] G.H. Liu, J.Y. Wang, T.Z. Huang, X.H. Liang, Y.L. Zhang, H.X. Li, J. Mater. Chem. 20 (2010) 1970.
[19] Y.Q. Sun, G.H. Liu, H.Y. Gu, T.Z. Huang, Y.L. Zhang, H.X. Li, Chem. Commun. 47 (2011) 2583.
[20] J. Long, G.H. Liu, T.Y. Cheng, H. Yao, Q.Q. Qian, J.L. Zhuang, F. Gao, H.X. Li, J. Catal. 298 (2013) 41.
[21] Y.L. Xu, J. Long, K.T. Liu, Q.Q. Qian, F. Gao, G.H. Liu, H.X. Li, Adv. Synth. Catal. 354 (2012) 3250.
[22] G.H. Liu, H.Y. Gu, Y.Q. Sun, J. Long, Y.L. Yu, H.X. Li, Adv. Synth. Catal. 353 (2011) 1317.
[23] R.H. Jin, K.T. Liu, D.Q. Xia, Q.Q. Qian, G.H. Liu, H.X. Li, Adv. Synth. Catal. 354 (2012) 3265.
[24] I. Yamada, R. Noyori, Org. Lett. 2 (2000) 3425.
[25] O. Krőcher, O.A. Kőppel, M. Frőba, A. Baiker, J. Catal. 178 (1998) 284.
[26] H.X. Li, Q.F. Zhao, Y. Wan, W.L. Dai, M.H. Qiao, J. Catal. 244 (2006) 251.
[27] T.L. Wang, L.G. Zhuo, Z.W. Li, F. Chen, Z.Y. Ding, Y.M. He, Q.H. Fan, J.F. Xiang, Z.X. Yu, A.S.C. Chan, J. Am. Chem. Soc. 133 (2011) 9878.
[28] P. Brant, T.A. Stephenson, Inorg. Chem. 26 (1987) 22.
[29] T.K. Maishal, J. Alauzun, J.M. Basset, C. Copéret, R.J.P. Corriu, E. Jeanneau, A. Mehdi, C. Reyé, L. Veyre, C. Thieuleux, Angew. Chem., Int. Ed. 47 (2008) 8654.
[30] I. Karamé, M. Boualleg, J.M. Camus, T.K. Maishal, J. Alauzun, J.M. Basset, C. Copéret, R.J.P. Corriu, E. Jeanneau, A. Mehdi, C. Reyé, L. Veyre, C. Thieuleux, Chem. Eur. J. 15 (2009) 11820–11823.
[31] T. Posset, J. Blumel, J. Am. Chem. Soc. 128 (2006) 8394.
[32] V. Cauda, A. Schlossbauer, J. Kecht, A. Zürner, T. Bein, J. Am. Chem. Soc. 131 (2009) 11361.
[33] F. Zaera, Chem. Soc. Rev. 42 (2013) 2746.
[34] C. del Pozo, A. Corma, M. Iglesias, F. Sánchez, Green Chem. 13 (2011) 2471.
[35] W.B. Lin, Top. Catal. 53 (2010) 869.
[36] P. Wang, X. Liu, J. Yang, Y. Yang, L. Zhang, Q.H. Yang, C. Li, J. Mater. Chem. 19 (2009) 80090.
[37] C. Wang, C.Q. Li, X.F. Wu, A. Pettman, J.L. Xiao, Angew. Chem. 121 (2009) 6646.
[38] D.S. Wang, Q.A. Chen, S.M. Lu, Y.G. Zhou, Chem. Rev. 112 (2012) 2557.